RSC Advances

ROYAL SOCIETY OF CHEMISTRY

www.rsc.org/advances

RSC Advances

ARTICLE

Core-shell structured Fe_3O_4@SiO_2@CdS nanoparticles with enhanced visible-light photocatalytic activities

Received 00th January 20xx,
Accepted 00th January 20xx

DOI: 10.1039/x0xx00000x

www.rsc.org/

Wen Shi,[a] Deli Lu,[b] Lingzhi Wang,[a]* FeiTeng[c] and Jinlong Zhang[a]*

Chelating-assistant growth route of CdS on the surface of Fe_3O_4@SiO_2 nanoparticles (NPs) was used to form magnetically recoverable photocatalyst. Characterizations by transmission electron microscopy, X-ray powder diffraction, Raman spectroscopy and vibrating sample magnetometer reveal monodispersed superparamagnetic Fe_3O_4@SiO_2@CdS NPs (250 nm) have been formed with a uniform CdS shell thickness of ca. 20 nm, Brunauer–Emmett–Teller (BET) surface area of ca. 25.1 $m^2 \cdot g^{-1}$ and saturation magnetization of 22.02 $emu \cdot g^{-1}$. This composite shows excellent photocatalytic activity towards the degradation of methylene blue (MB) under visiable-light irradiation with a reaction constant of 1.95×10^{-2} min^{-1} in spite of the low weight percentage of CdS (9.15%) as determined by the energy-dispersive X-ray spectroscopy, which is higher than those observed on Fe_3O_4@CdS (53.30%, 1.22×10^{-2} min^{-1}) and CdS NPs (3.33×10^{-3} min^{-1}). Furthermore, Fe_3O_4@SiO_2@CdS can be quickly magnetically recovered within 30 s by applying an external magnetic field near the solution after the photocatalytic process, which still preserves the excellent particle monodispersity with the slightly reduced CdS thickness (ca. 15 nm), while Fe_3O_4@CdS and CdS NPs are severely photo-corroded and aggregated. The maximized specific surface area from uniform coating and the efficient generation of activated oxygen species from CdS shells might be responsible for the enhanced photoactivity.

1. Introduction

Recently, magnetic core-shell NPs have attracted considerable attentions due to their essential applications in many fields such as photocatalysis[1-3], biomolecule enrichment[4, 5], Raman analysis[6, 7], pollutants adsorption[8, 9], fluorescent sensor[10, 11], drug transportation[12, 13], and bioimaging[14, 15]. Among them, the design and synthesis of magnetic photocatalysts with high performance have long been research hotspot due to the increasingly severe pollution situation. Up to now, magnetically separable photocatalysts using magnetite as the core and TiO_2[16], SnO_2[17], NiO[18], ZnO[19], and MnO_2[20] as the shell have been successfully synthesized. Concentrated efforts have been devoted to improve the coating quality to obtain highly dispersed magnetic photocatalyst[21, 22]. Meanwhile, other attention has been paid to improve the quantum yield[23] and extend the light absorption range of the photocatalyst[24].

Cadmium sulfide (CdS) with a direct band gap of 2.42 eV is a promising visible-light active semiconductor, which is of great importance in the area of environmental purification under visible light[25, 26]. Although there are some reports concerned with the magnetically recoverable CdS[27, 28], the problem of particle agglomeration during the growth of CdS have actually not been efficiently resolved. Anisotropic CdS/Fe_3O_4 dimer and loading type like CdS-Fe_3O_4 have been commonly observed[29-31]. However, uniform deposition of CdS layer to maximize the active surface is still difficult and remains a great challenge. The main reason may be the difficulty to control the reaction kinetics of two precursors (Cd, S) on Fe_3O_4 core, and the existence of surface tension and lattice mismatch between CdS and Fe_3O_4.

Herein, using hydrophilic Fe_3O_4@SiO_2 as the cores, we report the successful synthesis of Fe_3O_4@SiO_2@CdS NPs through a chelating-assistant growth route for the in-situ coating of CdS shell with trisodium citrate as the chelating agent. The core-shell NPs are highly monodispersed with a diameter of ca. 250 nm and a uniform CdS shell thickness of ca. 20 nm. When used for the photocatalytic degradation of MB, the Fe_3O_4@SiO_2@CdS NPs show excellent photocatalytic activity with a reaction constant of 1.95×10^{-2} min^{-1} under visible light irradiation, much higher than those observed on Fe_3O_4@CdS (1.22×10^{-2} min^{-1}) and CdS NPs (3.33×10^{-3} min^{-1}) with higher CdS content. The NPs can be easily magnetically recovered by applying an external magnetic field, which still preserves excellent monodispersity with a slightly reduced CdS thickness after the catalytic reaction. In comparison, Fe_3O_4@CdS and CdS NPs underwent severely photo-corrosion.

[a] Key Laboratory for Advanced Materials and Institute of Fine Chemicals, East China University of Science and Technology, 130 Meilong Road, Shanghai 200237, P. R. China E-mail address: wlz@ecust.edu.cn; jlzhang@ecust.edu.cn
[b] School of Chemical and Environmental Engineering, Shanghai Institute of Technology, Shanghai,201418, PR China
[c] Innovative Research Laboratory of Environment & Energy, Jiangsu Key Laboratory of Atmospheric Environment Monitoring & Pollution Control, School of Environmental Science and Engineering, Nanjing University of Information Science & Technology, P.R. China
Electronic Supplementary Information (ESI) available: [details of any supplementary information available should be included here]. See DOI: 10.1039/x0xx00000x

and particle aggregation. The high photocatalytic performance of Fe_3O_4@SiO_2@CdS NPs was also tested by degradation of antibiotic like tetracycline (TC) with high pollutant concentration. Possible reasons of enhanced photocatalytic activities were discussed in detail.

2. Experimental section

2.1 Materials

Ferric chloride hexahydrate ($FeCl_3 \cdot 6H_2O$), trisodium citrate dehydrate, sodium acetate, ethylene glycol, tetraethyl orthosilicate (TEOS), ammonia aqueous solution ($NH_3 \cdot H_2O$, 25 wt%), ethanol, thiourea, trisodium citrate, cadmium chloride ($CdCl_2$). All chemicals were of analytical grade, and they were used without further purification.

2.2 Preparation of photocatalysis

Synthesis of Fe_3O_4 NPs: The magnetic Fe_3O_4 NPs were prepared according to a solvothermal method reported previously[32]. In a typical synthesis, $FeCl_3 \cdot 6H_2O$ (0.86 g), trisodium citrate dehydrate (0.48 g), and sodium acetate (1.75 g) were dissolved in ethylene glycol (30 mL) under vigorous stirring. The obtained homogeneous yellow solution was transferred to a Teflon-lined stainless-steel autoclave (30 mL). The autoclave was heated to 200 °C and maintained for 10 h, and then, it was cooled down to room temperature. The obtained black magnetite particles were washed with water and ethanol for five times, respectively. The particles were conserved in the ethanol.

Synthesis of Fe_3O_4@SiO_2 core-shell NPs: Fe_3O_4@SiO_2 core-shell NPs were prepared according to a modified Stöber method[33]. Typically, the Fe_3O_4 NPs (50 mg) were dispersed in an ethanol (100 mL) and water (25 mL) solution, followed by the addition of ammonia aqueous solution (1.75 mL, 25 wt%) and TEOS (300 μL). After stirring at 25 °C for 12 h, the Fe_3O_4@SiO_2 NPs were obtained and washed five times with water and ethanol, respectively. The particles were conserved in the ethanol.

Synthesis of Fe_3O_4@SiO_2@CdS core-shell NPs: The Fe_3O_4@SiO_2 (25 mg) NPs were dispersed in water (50 mL), followed by addition of trisodium citrate (3 mL, 0.1 M) and $CdCl_2$ (5 mL, 0.05 M). Then, the pH of the suspension was adjusted to 10. Afterward, thiourea (1.3 mL, 0.2 M) was added and the result solution was put in a bath at 60 °C. The reaction was kept ultrasonic for 3 h. The resultant Fe_3O_4@SiO_2@CdS NPs were magnetically collected and washed with water and ethanol five times, respectively. The product was dried at 60 °C overnight in an oven.

Synthesis of Fe_3O_4@CdS and CdS NPs: Fe_3O_4@CdS core-shell NPs were prepared through in-situ coating of CdS onto the surface of Fe_3O_4 cores directly and CdS NPs were prepared in absent of Fe_3O_4@SiO_2 cores but other reagents and conditions being unchanged.

2.3 Characterizations

The crystal phases of the as-prepared samples were analyzed by XRD which were conducted to identify the samples' microstructure characteristics, were collected in the range of 5-80° (2θ) and recorded on a Rigaku D/MAX-2550 diffractometer using Cu Kα radiation of wavelength 1.5406 Å, typically running at a voltage of 40 kV and current of 100 mA. The transmission electron microscopy (TEM) was conducted on a JEOL JEM-2100EX electron microscope, operated at an accelerating voltage of 200 kV. The concentration of the pollutant was measured using a UV–vis spectrophotometer (Shimadzu, UV-2450). Raman measurements were performed at room temperature using a Via + Reflex Raman spectrometer with the excitation wavelength of 514 nm. The BET of the sample was determined through nitrogen adsorption at 77 K (Micromeritics ASAP 2010). The sample was degassed at 373 K before the measurement. The magnetic hysteresis loop was measured using a vibrating sample magnetometer (VSM, LakeShore 7407) at room temperature.

2.4 Photocatalytic experiments

To investigate the photocatalytic activities of the Fe_3O_4@SiO_2@CdS, Fe_3O_4@CdS and CdS NPs, methyl blue(MB) and tetracycline(TC) were chosen as the test molecules. In a typical procedure, 10 mg of the as-prepared NPs and 50 mL of 10 $mg \cdot L^{-1}$ MB and TC mother solution were used. The light source was a 1000 W tungsten-halide lamp (Philips) equipped with wavelength cutoff filters (λ > 420 nm) and focused on the beaker. Prior to irradiation, the suspension was ultrasonicated for 10 min and then stirred in dark for 30 min to achieve the adsorption/desorption equilibrium established. After turning on the lamp, three milliliters of the turbid solution was removed from the above solution at fixed time intervals and immediately magnetic separated. The upper clear liquid was analyzed by recording the characteristic absorption peak of MB at 664 nm and TC at 350 nm to calculate the concentration of the compounds.

3. Results and discussion

3.1 Synthesis and microstructure characterizations

The synthesis scheme of Fe_3O_4@SiO_2@CdS NPs is presented in Scheme. 1. Fe_3O_4 NP with diameter of ca. 130 nm was used as the core, which is pre-coated with a SiO_2 layer with thickness of ca. 40 nm. Chemical bath deposition (CBD) method was used to deposit CdS shell with trisodium citrate as the chelating agent and thiourea, $CdCl_2$ as the precursor.

Fig. 1a shows the TEM image of Fe_3O_4@SiO_2 cores with diameter of ca. 210 nm. Fe_3O_4@SiO_2@CdS NPs were obtained chelating agent for controlling the concentration of Cd, which helps releasing Cd^{2+} slowly to ensure the forming of

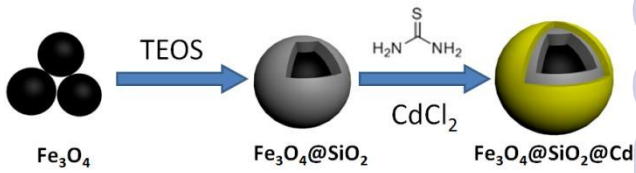

Scheme 1 Schematic illustration of the formation of the Fe_3O_4@SiO_2@CdS NPs

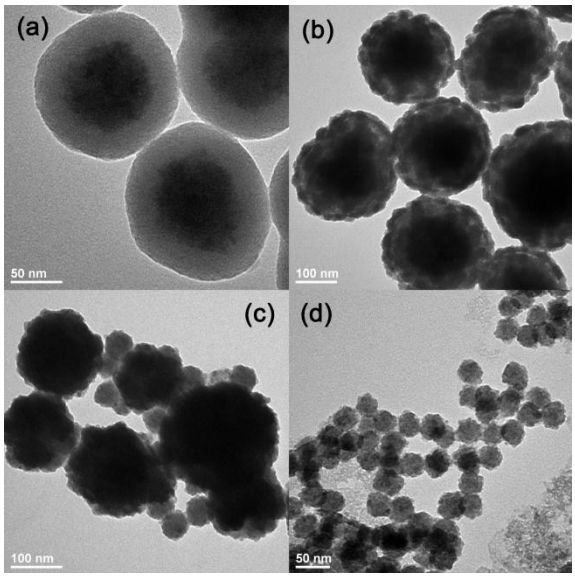

Fig. 1 TEM images of (a) Fe_3O_4@SiO_2, (b) Fe_3O_4@SiO_2@CdS, (c) Fe_3O_4@CdS and (d) CdS NPs.

after the coating of CdS. TEM images (Fig. 1b, S1) indicate the CdS shell is uniform with a thickness of ca. 20 nm. The direct coating of CdS on Fe_3O_4 leads to the formation of aggregated Fe_3O_4@CdS (Fig. 1c) with non-deposited CdS NPs formed from the homogenous nucleation, indicating the pre-coating of Fe_3O_4 with hydrophilic SiO_2 layer is necessary for the uniform coating of CdS shell, due to the attraction of Cd^{2+} by the negative charge on SiO_2 surface besides the adoption of uniform CdS shell instead of bulk CdS. Moreover, CdS NPs which were synthesized in the absence of magnetic core shows poor particle dispersibility with inhomogeneous particle sizes of 30 - 45 nm (Fig. 1d), which is commonly observed from the aqueous synthesis system due to the self-nucleation in a less controlled way. The magnetic property of the Fe_3O_4@SiO_2@CdS NPs was quantified by using a VSM at room temperature. The hysteresis loops are illustrated in Fig. 2 indicating that the as-prepared samples show negligible coercivity and remanence. The saturation magnetization (Ms) for Fe_3O_4@SiO_2@CdS NPs is about 22.02 emu·g^{-1} comparable to that of Fe_3O_4@SiO_2 (28.84 emu·g^{-1}). The little decrease in

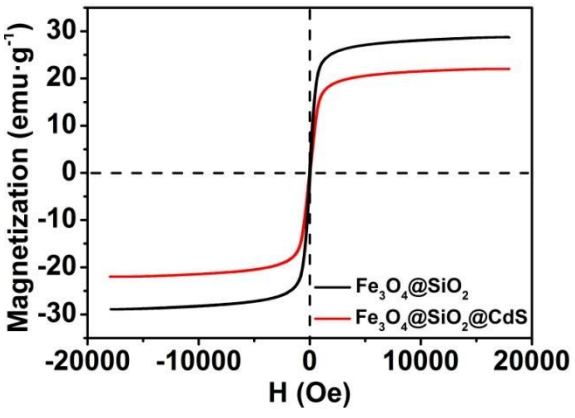

Fig. 2 Field-dependent magnetization curve of Fe_3O_4@SiO_2@CdS compared with Fe_3O_4@SiO_2 NPs at room temperature.

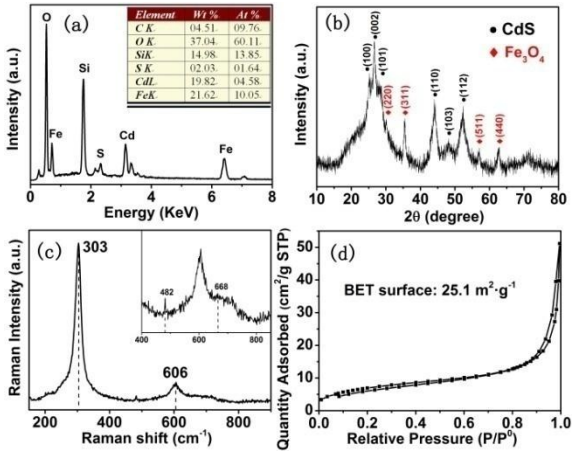

Fig. 3 (a) EDS patterns of Fe_3O_4@SiO_2@CdS NPs; (b) XRD patterns of Fe_3O_4@SiO_2@CdS NPs; (c) Raman spectra of Fe_3O_4@SiO_2@CdS NPs; (d) Nitrogen adsorption–desorption measurements and the estimated BET surface areas of the Fe_3O_4@SiO_2@CdS NPs.

Ms could be attributed to the introduction of nonmagnetic CdS shell, which increases the mass of the whole NP and quenches the magnetic moment[34]. Such parameter means that Fe_3O_4@SiO_2@CdS NPs have strong magnetic responsively thus can be easily separated from the solution by an external magnet field.

The EDS confirms the presence of O, Si, S, Cd and Fe elements in Fe_3O_4@SiO_2@CdS NPs (Fig. 3a). The wide-angle XRD patterns in Fig. 3b show distinct peaks at 2θ values of 25.2° (100), 26.7° (002), 43.7° (110), 48.1° (103) and 51.9° (112) indexing to the planes of hexagonal phase CdS (JCPDS Card No. 80-0006), indicating good crystallinity of CdS shell. Meanwhile, the characteristic peaks of orthorhombic phase Fe_3O_4 (JCPDS Card No. 19-0629) can also be found at the 2θ values of 30.1° (220), 35.5° (311), 57.1° (511) and 62.8° (440). The broad peaks observed at 2θ values of 21.6° are related to the amorphous SiO_2 (JCPDS Card No. 50-1432). Raman spectrum (Fig. 3c) demonstrates distinct peaks at 303 and 606 cm^{-1} corresponding to 1 LO (longitudinal optical) and 2 LO optical phonons in CdS NPs, respectively[35]. The fine peaks located in 482 and 668 cm^{-1} can be identified as T_{2g} and A_{1g} band of magnetite, respectively[36]. N_2 adsorption–desorption isotherm (Fig. 3d) shows typical type II curves ascribing to macroporous material. The BET surface area (S_{BET}) of Fe_3O_4@SiO_2@CdS NPs is determined to be 25.1 $m^2 \cdot g^{-1}$.

3.2 Photocatalytic properties

After examining the structure and magnetic property of the as-prepared NPs, we proceeded to evaluate the photocatalytic properties under visible light irradiation, using MB as the model contaminant. Fig. 4 shows the temporal evolution of the absorption spectra of the MB aqueous solution containing the Fe_3O_4@SiO_2@CdS NPs during the photocatalytic process. Before the photocatalytic process, the suspensions were ultrasonicated for 10 min and then stirred in dark for 30 min to achieve the adsorption/desorption

equilibrium established. Obviously, MB can hardly be absorbed by Fe_3O_4@SiO_2@CdS NPs. With the prolonging irradiation time,

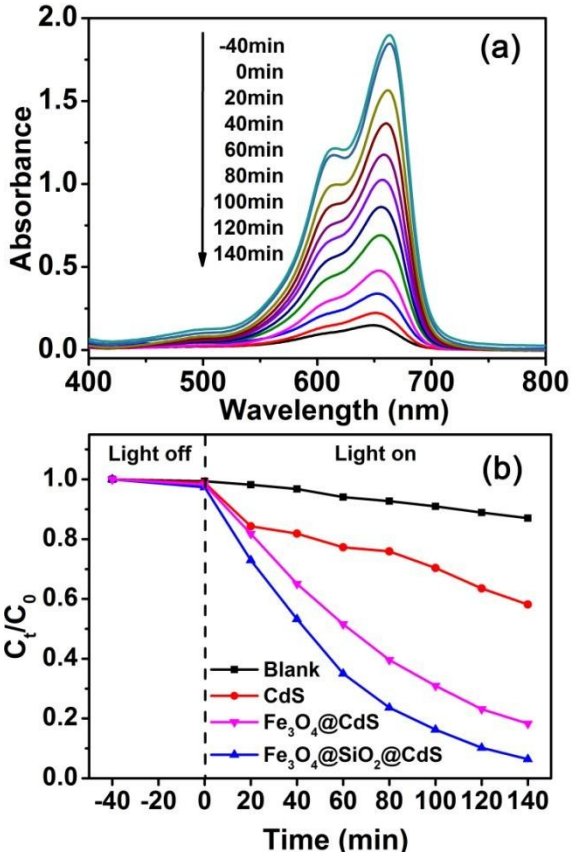

Fig. 4 (a) Absorption spectra of the solution of MB exposed to irradiation for different time in the presence of Fe_3O_4@SiO_2@CdS NPs as photocatalyst. (b) Photocatalytic performances of the as-prepared samples under visible light irradiation.

the absorption peak at 664 nm decreased rapidly indicating the degradation of MB.

As can be seen in Fig. 4b, about 94% of MB was degraded within 140 min. In comparison, Fe_3O_4@CdS and CdS NPs with the same particle dosage show 81% and 42% of degradation rates. This result indicates the coating type CdS no matter for Fe_3O_4@CdS or Fe_3O_4@SiO_2@CdS indeed possesses superior activity to the single CdS NPs. Moreover, according to the statistics in tables of EDS images, the actual weight percentages of CdS were calculated (see methods in supporting information). Since the Fe_3O_4@SiO_2@CdS NPs (9.15%, Fig. 3a) show the least amount of CdS compared with Fe_3O_4@CdS (53.30%, Fig. S2) and CdS NPs, the actual photocatalytic activity should be more superior. Furthermore, benefitted from the superparamagnetic property of Fe_3O_4@SiO_2@CdS, the photocatalyst can be recycled within 30 s by applying an external magnetic field (8000 GS) near the solution after the photocatalytic process (Fig. S3), which is in accordance with the good magnetic property.

In order to quantitatively determine the degradations rates of MB over different photocatalysts, the degradation curves are further expressed by the pseudo-first order model as follows:

$$\ln(C_0/C_t)=kt$$

where C_0 and C_t are the concentrations of MB in the solution at time 0 and t, respectively, and k is the pseudo-first

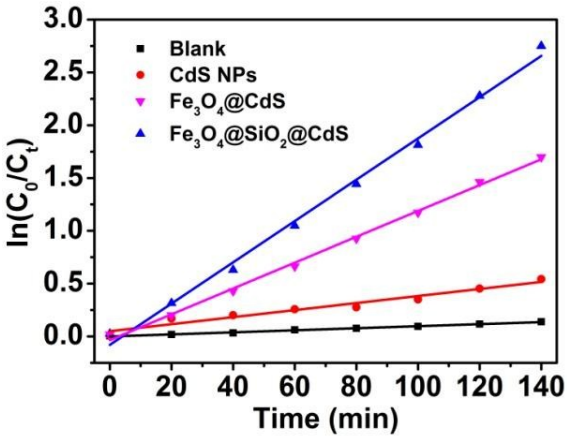

Fig. 5 Pseudo-first order plots of MB in the solutions containing the as-prepared samples under visible light.

order rate constant. Fig. 5 shows the plots of $\ln(C_0/C_t)=kt$ versus the irradiation time for the photodegradation of MB. The result suggests the good fitting of all the degradation process by pseudo-first order model. The reaction constant value of Fe_3O_4@SiO_2@CdS is calculated to be 1.95×10^{-2} min^{-1}, much higher than those of Fe_3O_4@CdS (1.22×10^{-2} min^{-1}) and CdS NPs (3.33×10^{-3} min^{-1}).

For further testing the high activity of Fe_3O_4@SiO_2@CdS, tetracycline (TC), a very stable antibiotic with the maximum absorption peak at 357 nm, was also chosen as the model contaminant for photocatalytic degradation under visible light irradiation (λ > 420 nm). Fig. 6 shows the change of the absorption spectra of a TC aqueous solution (100 mg•L^{-1}, 50 mL) in the presence of 10 mg of the catalyst. It can be seen that over 20% of TC was adsorbed in 20 min and the degradation ratio reached to 80% just within 21 min in such a high concentration of pollutant, which indicated the high photocatalytic performance of the Fe_3O_4@SiO_2@CdS NPs. Since the maximum peak of TC is 357 nm lower than 420 nm, it ruled out the possibility of dye-sensitization at the same time.

Based on the above results, the improved photocatalytic activity of Fe_3O_4@SiO_2@CdS NPs should be related to the maximized active sites due to the uniformly coated structure

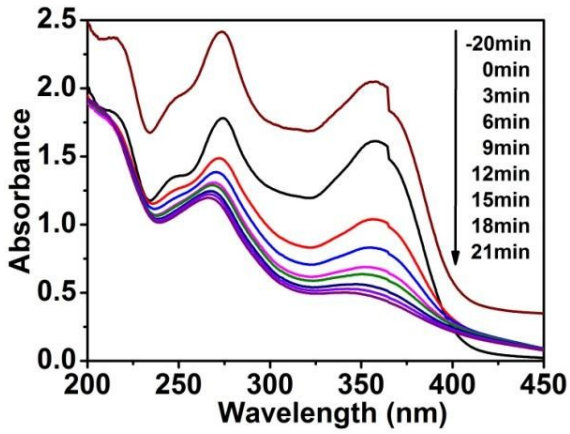

Fig. 6 Absorption spectra of the solution of TC exposed to irradiation for different time in the presence of Fe_3O_4@SiO_2@CdS NPs as photocatalyst.

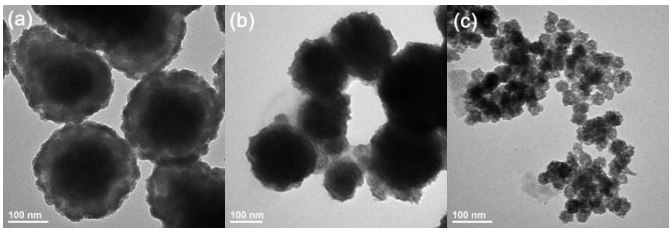

Fig. 7 TEM images of (a) Fe_3O_4@SiO_2@CdS, (b) Fe_3O_4@CdS and (c) CdS NPs after photocatalytic tests for 140 min.

together with the excellent particle dispersibility and the efficient generation of activated oxygen species from CdS shells due to an electronic semiconductor-support interaction mediated through surface [Si]-O-Cd-S bonds[37, 38]. Moreover, the structures of Fe_3O_4@SiO_2@CdS, Fe_3O_4@CdS and CdS NPs after the photocatalytic degradation of MB were further analyzed by TEM to understand the structure stability. As seen from Fig. 7a, the recovered Fe_3O_4@SiO_2@CdS NPs still owned core-shell structured morphology. The thickness of CdS shell showed slight decrease from 20 to 15 nm. In comparison, the CdS NPs suffered severe agglomeration and the thin CdS shell on Fe_3O_4@CdS almost disappeared (Fig. 7b, 7c). These results clearly demonstrated that the active sites on Fe_3O_4@SiO_2@CdS were better preserved during the photocatalytic process, which should also contribute to the enhanced photocatalytic activity.

4. Conclusions

Core-shell structured Fe_3O_4@SiO_2@CdS NPs have been successfully synthesized through a chelating-assistant growth route for the in-situ coating of CdS shell using trisodium citrate as the chelating agent. The obtained NPs are monodispersed with a diameter of ca. 250 nm and a uniform CdS shell of ca. 20 nm. Photocatalytic tests demonstrate the Fe_3O_4@SiO_2@CdS NPs own excellent photocatalytic activity towards the degradation of MB compared with Fe_3O_4@CdS and CdS NPs. Further study shows the reaction rates well fit the pseudo-first order model, Fe_3O_4@SiO_2@CdS NPs have the top reaction constant value of 1.95×10^{-2} min^{-1}, much higher than those observed on Fe_3O_4@CdS (1.22×10^{-2} min^{-1}) and CdS NPs (3.33×10^{-3} min^{-1}). Another test also demonstrates that Fe_3O_4@SiO_2@CdS NPs show a high photocatalytic performance of degradation of antibiotic like TC. The high photoactivity mainly results from the uniform coating and the efficient generation of activated oxygen species from CdS shell. The improved photocatalytic performance and photo-stability of CdS through uniform coating strategy provides more opportunity for the application of quantum dots in the environment and energy fields.

Conflict of interest

The authors declare no competing financial interest.

Acknowledgements

This work has been supported by National Nature Science Foundation of China (U1407102, 21237003 and 21377038), the National Basic Research Program of China (973 Program, 2013CB632403), the Science and Technology Commission of Shanghai Municipality (14ZR1410700, 14230710500), PetroChina Innovation Foundation 2015D-5006-0402, the Research Fund for the Doctoral Program of Higher Education (20120074130001), the Fundamental Research Funds for the Central Universities, Open Project from Jiangsu Key Laboratory of Atmospheric Environment Monitoring and Pollution Control of Nanjing University of Information Science and Technology (kHK1110) and Jiangsu Province Innovation Platform for Superiority Subject of Environmental Science and Engineering.

References

1. B. Tian, R. Dong, J. Zhang, S. Bao, F. Yang and J. Zhang, *Applied Catalysis B: Environmental*, 2014, **158**, 76-84.
2. X. Dong, Y. Shao, X. Zhang, H. Ma, X. Zhang, F. Shi, C. Ma and M. Xue, *Research on Chemical Intermediates*, 2014, **40**, 2953-2961.
3. J.-W. Xu, Z.-D. Gao, K. Han, Y. Liu and Y.-Y. Song, *ACS applied materials & interfaces*, 2014, **6**, 15122-15131.
4. W. Ma, Y. Zhang, L. Li, Y. Zhang, M. Yu, J. Guo, H. Lu and C. Wang, *Advanced Functional Materials*, 2013, **23**, 107-115.
5. W.-F. Ma, Y. Zhang, L.-L. Li, L.-J. You, P. Zhang, Y.-T. Zhang, J.-M. Li, M. Yu, J. Guo and H.-J. Lu, *ACS nano*, 2012, **6**, 3179-3188.
6. X. Zhang, Y. Zhu, X. Yang, Y. Zhou, Y. Yao and C. Li, *Nanoscale*, 2014, **6**, 5971-5979.
7. J. Du and C. Jing, *The Journal of Physical Chemistry C*, 2011, **115**, 17829-17835.
8. T. Wang, L. Zhang, C. Li, W. Yang, T. Song, C. Tang, Y. Meng, S. Dai, H. Wang and L. Chai, *Environmental science & technology*, 2015, **49**, 5654-5662.
9. X. Tan, L. Lu, L. Wang and J. Zhang, *European Journal of Inorganic Chemistry*, 2015.
10. S. Mohapatra, S. Sahu, S. Nayak and S. K. Ghosh, *Langmuir*, 2015, **31**, 8111-8120.

11. D. Lu, F. Teng, Y. Liu, L. Lu, C. Chen, J. Lei, L. Wang and J. Zhang, *RSC Advances*, 2014, **4**, 18660-18667.
12. J. Lei, L. Wang and J. Zhang, *ACS Nano*, 2011, **5**, 3447-3455.
13. H. Qiu, B. Cui, G. Li, J. Yang, H. Peng, Y. Wang, N. Li, R. Gao, Z. Chang and Y. Wang, *The Journal of Physical Chemistry C*, 2014, **118**, 14929-14937.
14. Y. Lu, B. He, J. Shen, J. Li, W. Yang and M. Yin, *Nanoscale*, 2015, **7**, 1606-1609.
15. L.-S. Lin, Z.-X. Cong, J.-B. Cao, K.-M. Ke, Q.-L. Peng, J. Gao, H.-H. Yang, G. Liu and X. Chen, *ACS nano*, 2014, **8**, 3876-3883.
16. J. Lan, *Research on Chemical Intermediates*, **41**, 3531-3541.
17. R. Li, X. Ren, F. Zhang, C. Du and J. Liu, *Chemical Communications*, 2012, **48**, 5010-5012.
18. T. Li, C. Yang, X. Rao, F. Xiao, J. Wang and X. Su, *Ceramics International*, 2015, **41**, 2214-2220.
19. J. Wan, H. Li and K. Chen, *Materials Chemistry and Physics*, 2009, **114**, 30-32.
20. J. Liu, Z. Zhao, P. Shao and F. Cui, *Chemical Engineering Journal*, 2015, **262**, 854-861.
21. R. Chalasani and S. Vasudevan, *ACS nano*, 2013, **7**, 4093-4104.
22. A. Hasanpour, M. Niyaifar, H. Mohammadpour and J. Amighian, *Journal of Physics and Chemistry of Solids*, 2012, **73**, 1066-1070.
23. X. Li, D. Liu, S. Song and H. Zhang, *Crystal Growth & Design*, 2014, **14**, 5506-5511.
24. Q. Zhang, G. Meng, J. Wu, D. Li and Z. Liu, *Optical Materials*, 2015.
25. Y. P. Xie, Z. B. Yu, G. Liu, X. L. Ma and H.-M. Cheng, *Energy & Environmental Science*, 2014, **7**, 1895-1901.
26. K. Zhao, Z. Wu, R. Tang, Y. Jiang and Y. Lu, *Research on Chemical Intermediates*, 2014, 1-7.
27. X. Liu, Z. Fang, X. Zhang, W. Zhang, X. Wei and B. Geng, *Crystal Growth and Design*, 2008, **9**, 197-202.
28. A. Roychowdhury, S. P. Pati, S. Kumar and D. Das, *Materials Chemistry and Physics*, 2015, **151**, 105-111.
29. H. McDaniel and M. Shim, *ACS nano*, 2009, **3**, 434-440.
30. L. Wang, H. Wei, Y. Fan, X. Gu and J. Zhan, *The Journal of Physical Chemistry C*, 2009, **113**, 14119-14125.
31. Y. Liu, T. Yan, Y. Li, W. Cao, X. Pang, D. Wu and Q. Wei, *RSC Advances*, 2015, **5**, 19581-19586.
32. J. Liu, Z. Sun, Y. Deng, Y. Zou, C. Li, X. Guo, L. Xiong, Y. Gao, F. Li and D. Zhao, *Angewandte Chemie*, 2009, **121**, 5989-5993.
33. W. Stöber, A. Fink and E. Bohn, *Journal of colloid and interface science*, 1968, **26**, 62-69.
34. G. Liu, F. He, J. Zhang, L. Li, F. Li, L. Chen and Y. Huang, *Applied Catalysis B: Environmental*, 2014, **150**, 515-522.
35. R. R. Prabhu and M. A. Khadar, *Bulletin of Materials Science*, 2008, **31**, 511-515.
36. O. N. Shebanova and P. Lazor, *Journal of Solid State Chemistry*, 2003, **174**, 424-430.
37. H. Weiß, A. Fernandez and H. Kisch, *Angewandte Chemie International Edition*, 2001, **40**, 3825-3827.
38. J.-L. Hu, Q.-H. Yang, H. Lin, Y.-P. Ye, Q. He, J.-N. Zhang and H.-S. Qian, *Nanoscale*, 2013, **5**, 6327-6332.

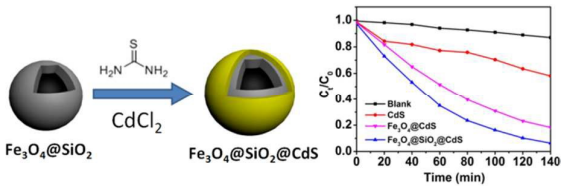

Uniform core-shell structured $Fe_3O_4@SiO_2@CdS$ is synthesized by a facile chelating-assistant growth route, which enhances the photocatalytic activities.